New Journal of Physics
The open-access journal for physics

Absolute frequency measurement of the $^2S_{1/2}$–$^2F_{7/2}$ electric octupole transition in a single ion of $^{171}Yb^+$ with 10^{-15} fractional uncertainty

S A King[1,2,3], R M Godun[1], S A Webster[1], H S Margolis[1], L A M Johnson[1], K Szymaniec[1], P E G Baird[2] and P Gill[1,2]

[1] National Physical Laboratory, Hampton Road, Teddington, TW11 0LW, UK
[2] Clarendon Laboratory, University of Oxford, Parks Road, Oxford OX1 3PU, UK
E-mail: steven.king@npl.co.uk

New Journal of Physics **14** (2012) 013045 (13pp)
Received 23 September 2011
Published 23 January 2012
Online at http://www.njp.org/
doi:10.1088/1367-2630/14/1/013045

Abstract. An absolute frequency measurement has been made of the $^2S_{1/2}$–$^2F_{7/2}$ electric octupole transition in a single ion of $^{171}Yb^+$. The implementation of a diode-based probe laser stabilized to this highly forbidden transition has resulted in an improvement of more than one order of magnitude upon the lowest published uncertainty. After correcting for systematic shifts, the frequency was determined to be 642 121 496 772 646.22 (67) Hz. This corresponds to a fractional uncertainty of 1.0×10^{-15}.

Contents

[3] Author to whom any correspondence should be addressed.

1. Introduction

Optical frequency standards offer the possibility of making a step improvement of more than two orders of magnitude in the stability and accuracy of the realization of the SI second. Improvements in laser technology and high-finesse Fabry–Perot cavities have allowed the development of ultrastable laser systems with frequency instabilities below 1×10^{-15} at averaging times from 1 to 30 s [1, 2]. These lasers can be used to interrogate highly forbidden optical reference transitions with the resulting quality factors approaching 10^{15}. Candidates for optical frequency standards based on single trapped ions or neutral atoms confined in optical lattice potentials are being investigated worldwide [3]. Systems based on single ions tightly confined in radio-frequency (rf) potentials have the advantage of a generally more uniform and easily characterized environment than is possible with their neutral atom counterparts. Systems based on Ca^+ [4–6], Yb^+ [7, 8], Sr^+ [9–11], Hg^+ [12], In^+ [13, 14] and Al^+ [15] are being developed and are continuously improving, with systematic uncertainties of below 1×10^{-17} being reported in the case of Al^+.

Ytterbium is unique among the ions being investigated as optical frequency standards in that its lowest-lying excited state is $^2F_{7/2}$ (see figure 1). Once populated, this state can only decay to the ground state via electric octupole (E3) radiation at 467 nm with a natural lifetime of about 6 years [16]. This leads to the $^2S_{1/2}$–$^2F_{7/2}$ transition possessing an extremely narrow natural linewidth of the order of nHz, resulting in a resolvable transition linewidth that depends primarily on the linewidth of the probe laser used to interrogate the transition. As the reference cavities used for probe laser stabilization continue to improve, so will the achievable short-term stability of the standard.

The octupole transition also has the smallest known quadrupole shift coefficient of any alkali-like ion [17], and the $m_F = 0 \rightarrow m_{F'} = 0$ component possesses zero linear Zeeman shift and a very low second-order Zeeman shift coefficient [18].

In addition to being of interest as a frequency standard, $^{171}Yb^+$ lends itself to tests of fundamental physics. The $^2S_{1/2}$–$^2D_{3/2}$ electric quadrupole (E2) transition at 436 nm offers another clock transition with a natural linewidth of 3.1 Hz. Two independent absolute frequency measurements of this transition are in good agreement [7, 19], and it is already accepted as a secondary representation of the SI second [20]. The ratio between the frequency of this transition and that of the octupole transition is highly sensitive to any temporal change in the fine structure constant, α [21–23]. The present limit to this time variation comes from high-accuracy comparisons of Al^+ and Hg^+ optical clocks at NIST [24].

In this paper, an improved absolute measurement of the octupole transition frequency is reported. The experimental setup, focusing on upgrades that have been made since the previous measurement, is discussed in section 2. An evaluation of all the systematic shifts associated with the transition that have uncertainties greater than 10^{-17} is contained in section 3. Section 4 presents a summary and outlook for the experiment. The total relative standard uncertainty, including both systematic and statistical contributions, is evaluated to be 1.0×10^{-15}, representing an improvement of a factor of 20 on the previously published value for this transition [8].

2. Experimental setup

A single ion of $^{171}Yb^+$ is confined in an rf endcap trap [25]. This design allows easy access for multiple cooling beams, allowing three-dimensional (3D) compensation of the ion's excess

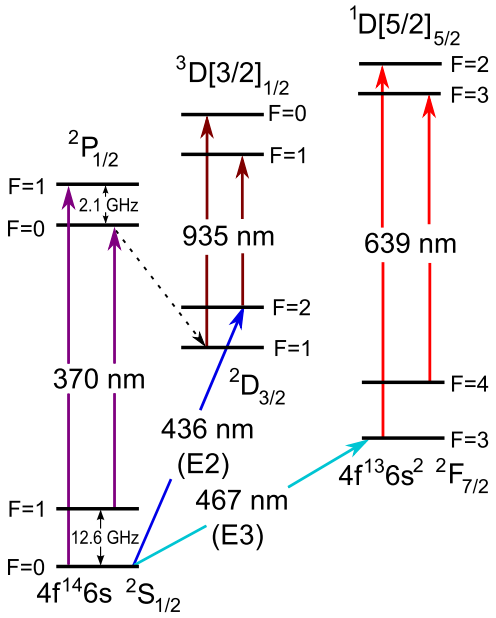

Figure 1. Simplified term scheme of $^{171}Yb^+$ showing the electric octupole (E3) transition at 467 nm and electric quadrupole (E2) transition at 436 nm.

micromotion. Loading is performed by heating an oven of isotopically enriched ^{171}Yb to produce an atomic beam. The $^1S_0$–$^1P_1$ transition in the neutral atoms is driven by a laser diode at 399 nm, and ionization is completed by light at the ion fluorescence wavelength of 370 nm produced by an Ar^+-pumped Ti:sapphire laser resonantly doubled in lithium triborate (LiB_3O_5). Once ionized, the ion is Doppler cooled by light red-detuned to the half-maximum of the strong $^2S_{1/2}$ $(F = 1) \rightarrow {}^2P_{1/2}$ $(F' = 0)$ transition at 370 nm (see figure 1) and fluorescence from the spontaneous decay from the $^2P_{1/2}$ state is monitored using a photomultiplier tube. Previously [8], a single π-polarized cooling beam was used and a magnetic field of around 300 μT destabilized the dark $m_F = \pm 1$ components of the ground state. If present during the probe phase of the clock cycle, this large field would induce a large and potentially unstable second-order Zeeman shift on the clock transition. It was therefore switched off to leave a small residual field to define the ion's quantization axis (which is determined using a well-calibrated orthogonal set of field coils driven by stable current supplies). The decay of the field to a suitable level was limited to a few tens of milliseconds, constituting a large fraction of the dead time within the clock cycle. This has since been replaced by a technique involving the simultaneous application of two cooling beams with an angular separation of 45° in their propagation vectors. The polarization of one beam is rapidly rotated between σ^-, π and σ^+ by an electro-optic modulator (EOM) operating near 2 MHz, and the second beam has a fixed π-polarization. This arrangement prevents coherent population trapping in the ground state by introducing a time-dependent relative phase between the three polarizations [26]. The minimum field is limited to about 20μT in order to avoid similar fluorescence nulls on the 935 nm transitions.

To prevent optical pumping to $^2S_{1/2}$ $(F = 0)$ arising from off-resonant excitation of the $F = 1 \rightarrow F' = 1$ component of the 370 nm transition, the $^2S_{1/2}$ $(F = 0) \rightarrow {}^2P_{1/2}$ $(F' = 1)$ transition is driven by the second-order sideband applied by a resonant EOM operating at 7.35 GHz. This has replaced the previous arrangement [8], which involved applying microwaves

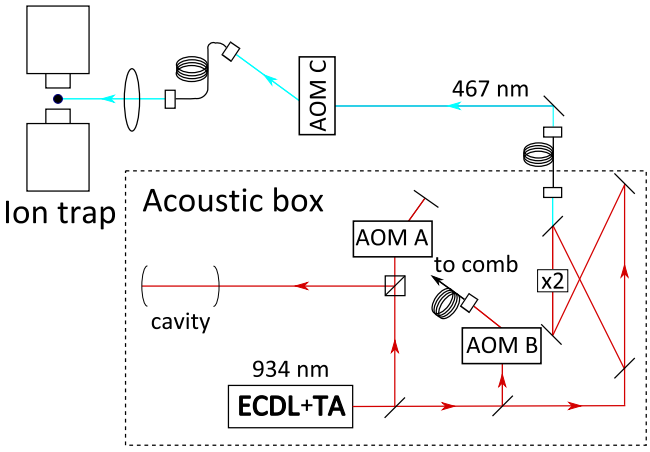

Figure 2. Simplified schematic of the experimental setup, showing the 934 nm ECDL, tapered amplifer (TA) and resonant frequency doubling to the probe wavelength of 467 nm. The key AOMs are illustrated that (A) offset the laser from the cavity mode, (B) provide drift compensation for the light sent to the frequency comb and (C) lock the laser to the atomic transition. The majority of the optics is contained within an acoustic box, from which the light is delivered to the trap via optical fibre.

at 12.6 GHz to mix the hyperfine levels of the ground state. Two diode lasers at 935 nm are used to depopulate the two hyperfine components of the metastable $^2D_{3/2}$ level, which are accessible via spontaneous decay from the $^2P_{1/2}$ level with a branching ratio of 7×10^{-3}. Similarly, two diode lasers at 639 nm are used to depopulate the $^2F_{7/2}$ level after excitation of the 467 nm transition or a decay into this state from the $^2D_{5/2}$ level after a collisional excitation from the $^2D_{3/2}$ level. With continuous laser cooling and all repumper wavelengths present, ion storage times of about a month are achieved. Without laser cooling, ions are typically lost from the trap after 6 h.

The clock laser setup is shown in figure 2. Light at 934 nm is produced by a commercial amplified external cavity diode laser (ECDL), which has recently replaced an Ar^+-pumped Ti:sapphire laser. Frequency sidebands at 1.9 MHz are added to the laser by a resonant EOM in order to stabilize the laser to an ultra-low-expansivity (ULE) Fabry–Perot etalon using the Pound–Drever–Hall (PDH) technique [27]. This modulation frequency was chosen to minimize the impact of any parasitic etalons in the beam path, whilst not restricting the achievable lock bandwidth [28]. The servo possesses two integral stages, one proportional stage and one differential stage. The lock bandwidth is limited to 200 kHz by the phase-lag in the response of the laser diode at high frequencies. A calcite polarizer with a 10^5:1 extinction ratio is used before the EOM to ensure a pure input polarization along the crystal axis, minimizing any amplitude modulation at the drive frequency. The ULE etalon has a finesse of 2×10^5 and is of a vibration-insensitive design [29]. It is mounted in vacuum and controlled within 1 K of the temperature at which its coefficient of thermal expansivity crosses zero (276 K) by dual-layer temperature control. The temperature stability of the heat shield internal to the vacuum chamber is measured to be about 100 μK over several hours. In order to produce the probe light at 467 nm, the laser is resonantly doubled in potassium niobate ($KNbO_3$). 80 mW of 467 nm radiation is typically

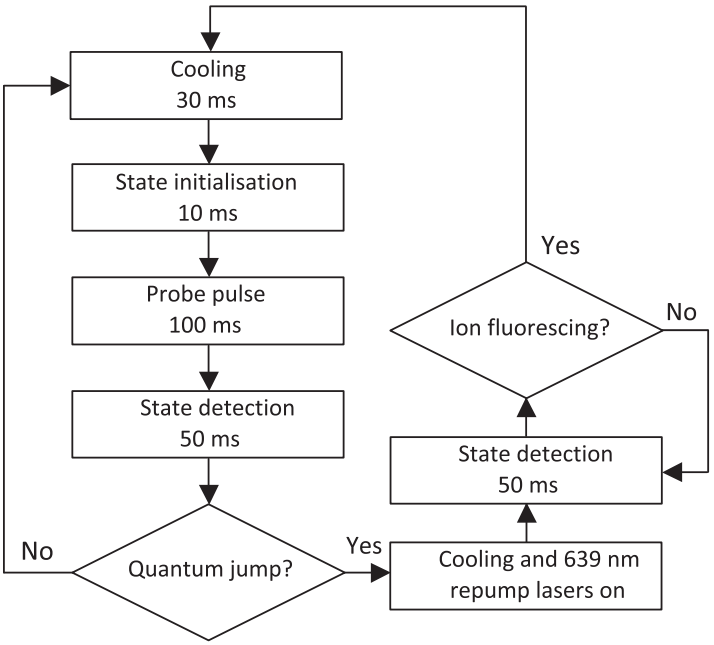

Figure 3. Depiction of the experimental sequence. If no fluorescence is detected after the probe phase, the bin is marked as a quantum jump and the 639 nm repumper lasers are applied. Repeated measurements of the state of the ion are made until a fluorescence signal is detected, at which point the sequence is reset. Typically only one repump phase is required. The sequence runs 20 times at each probe laser frequency in order to determine an excitation probability.

produced from a fundamental power of 400 mW. As the probe laser frequency associated with the mode of the cavity does not exactly coincide with the atomic resonance, a fixed frequency offset is introduced using AOM A in figure 2. The majority of the probe laser optics is mounted on an active vibration isolation platform enclosed within a wooden box lined with rubber and foam, providing isolation from acoustic noise and air currents. Light is delivered to the ion trap via optical fibre and focused to an adjustable beam waist at the ion.

The experimental sequence is depicted in figure 3. Before probing, the ion is initialized in the $^2S_{1/2}$ ($F = 0$) level by driving the $F = 1 \rightarrow F' = 1$ component of the 370 nm transition. Light at this frequency is generated by strongly modulating the 370 nm ($F = 1 \rightarrow F' = 0$) light at the hyperfine splitting frequency of the $^2P_{1/2}$ level using a second resonant EOM operating at 2.1 GHz. This rapidly pumps the ion to the desired state via $^2P_{1/2}$ ($F = 1$). Previously [8], state initialization was achieved by removal of the 12.6 GHz microwaves and waiting for an off-resonant excitation of the $F = 1 \rightarrow F' = 1$ transition.

A pulse of 467 nm probe light with 100 ms duration is then applied and subsequently the ion's state is detected by re-applying the 370 nm cooling light. Observation of fluorescence indicates a lack of excitation and the sequence is reset. If the ion remains dark, a quantum jump [30] to the $^2F_{7/2}$ state has occurred and the 639 nm lasers are applied to repump the ion to the ground state. The sequence is only restarted once fluorescence is detected.

Figure 4 shows a typical scan over the clock transition. The observed transition lineshape is a convolution of the laser lineshape on the timescale of the scan (about 1 min) with the Fourier

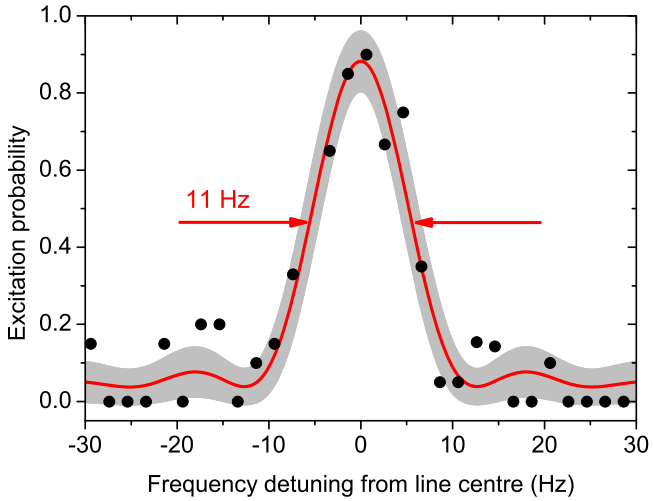

Figure 4. Typical scan over the octupole transition with a probe time of 100 ms. A lineshape has been fitted in accordance with the rectangular nature of the probe pulse, showing a linewidth close to the Fourier limit of 9 Hz. The shaded area indicates the predicted quantum projection noise.

transform-limited lineshape for the 100 ms probe duration. Under the assumption that both lineshapes are Lorentzian, the observed linewidth can be expressed as the linear sum of two individual linewidths, leading to an approximate laser linewidth of 2 Hz on this timescale.

To stabilize the clock laser to the forbidden transition, 20 interrogations are made on the high and low sides of the absorption line with a frequency separation given by the full-width at half-maximum. An acousto-optic modulator (AOM C in figure 2) is employed to step between the two probe frequencies. The excitation probabilities on the high and low frequency sides of the line (denoted by p_+ and p_-, respectively) are used to produce an error signal, e:

$$e = \frac{p_+ - p_-}{p_+ + p_-}. \tag{1}$$

This signal is then fed to a doubly integrating servo to steer the probe light back onto the line centre using AOM C, thus correcting for the drift of the ULE cavity:

$$\nu_{n+1} = \nu_n + G_1 \mathrm{e}_n + G_2(\Delta t) \sum_{i=0}^{n} \mathrm{e}_i, \tag{2}$$

where ν_n and ν_{n+1} are the probe laser frequencies before and after correction, respectively, and Δt is the time elapsed since the previous correction. This explicit time dependence is necessary as each complete lock cycle differs in length due to variations in the number of quantum jumps and hence the number of necessary repump phases. Optimum values for the gain coefficients G_1 and G_2 were found by a combination of modelling the response of the servo to quantum projection noise [31] and experimental investigations into the lock stability. It is this active stabilization of the probe laser frequency that allows greatly reduced statistical uncertainties compared to the previous measurement, in which the laser frequency was simply scanned across the line profile [8], resulting in low data rates and introducing uncertainties attributable to the line profile fit.

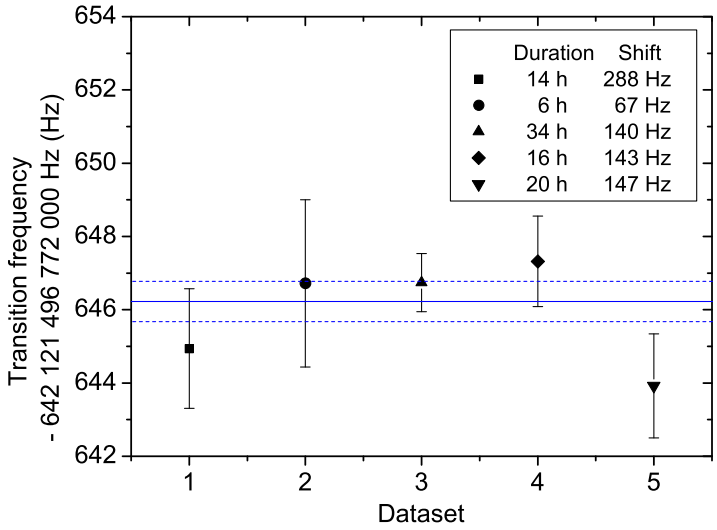

Figure 5. Summary of the data taken during July 2011. The legend shows the duration of each dataset and the differential scalar ac-Stark shift between the high and low power probe phases. A higher differential ac-Stark shift indicates a more focused probe beam. Error bars are one standard deviation and include statistical contributions only. The weighted mean and associated uncertainty are shown by solid and dashed lines, respectively.

In the previous measurement [8], the drive frequency of AOM C was recorded and combined in post-processing with data from the frequency comb. This approach relied on good synchronization of the computer systems in the ion and comb laboratories. The need for synchronization has since been eliminated. After each servo iteration, a correction is also made to the drive frequency of AOM B (between the probe laser and the frequency comb) that corresponds to the correction made by AOM C. The comb then measures a frequency that is offset from the current best estimate of the centre of the clock transition by a fixed value determined by the AOM drive frequencies.

The absolute frequency of the probe laser was measured using two femtosecond optical frequency combs, one based on a mode-locked Ti:sapphire laser [32, 33] and one based on an erbium-doped fibre laser [34]. The two combs were used to provide a cross-check for the values determined by each single comb. The two combs and the drive frequencies of AOMs A, B and C were referenced to one of the NPL hydrogen masers, the frequency of which was calibrated throughout the measurement period using the local caesium fountain primary standard NPL-CsF2 [35, 36].

3. Data and analysis

In order to measure the absolute frequency of the transition at the 10^{-15} level, the clock laser must be stabilized to the ion's transition for many hours and the data from the caesium fountain averaged for this period to reduce its statistical uncertainty. All systematic shifts of the transition frequency must also be determined and corrected for. A summary of the data after correction for systematic shifts is shown in figure 5.

The largest systematic shift of the 467 nm transition is the ac-Stark shift arising from the off-resonant coupling of the probe laser to other optical transitions from the two states involved in the clock transition, with the magnitude of the shift being directly proportional to the optical intensity at the ion. This shift was compensated for during the absolute measurement of the transition frequency. The laser was stepped between two power levels P_1 and P_2 (approximately 4 and 8 mW) and the two perturbed transition frequencies f_1 and f_2 were repeatedly measured by the optical frequency comb for periods of 20 min each. The unperturbed frequency f_0 can then be evaluated through

$$f_0 = f_2 - \frac{(f_2 - f_1)}{(1 - I_1/I_2)}, \tag{3}$$

where I_1 and I_2 are the laser intensities at the low and high power settings, respectively. By assuming a constant spot size for the laser over each extrapolation period of 40 min, the ratio I_1/I_2 is the same as the ratio of the two optical powers. This means it is not necessary to measure the spot size accurately, nor the optical power, but rather to determine the ratio between the two powers with high precision using a calibrated photodetector.

The probe beam can be focused to a $1/e^2$ radius of 5 μm at the ion using a multi-element lens array. During operation the laser was defocused to increase the beam size at the ion and hence reduce the effect of any drift in beam alignment, which would cause a varying intensity on the ion. Five different beam radii between 16 and 34 μm were used to allow the extrapolation to zero intensity to be carried out for different magnitudes of the ac-Stark shift, while maintaining a constant intensity ratio I_1/I_2 by choosing to operate with the same two power levels throughout.

The probe laser power is stabilized from shot to shot by using a photodiode to monitor a small pick-off of the light sent to the trap and then comparing this against a stable reference voltage to produce an error signal. This error signal is fed to an integrator and the correction applied to the drive power of AOM C. The resulting probe power has a fractional instability of 3×10^{-4} at high power and 7×10^{-4} at low power. The uncertainty on the extrapolation to zero intensity is dominated by how accurately the ratio between the two probe powers can be determined. The uncertainty on this figure is largely due to the instability of the probe power itself, but also includes contributions from the resolution and linearity of the detector used for the power measurement and the 2 ms capture time of the power servo, which must be activated each time the probe pulse begins.

The electric quadrupole shift $\Delta\nu_{\mathrm{quad}}$ arising from the interaction of stray dc electric field gradients with the electric quadrupole moment of the upper level of the clock transition is a function of the angle β between the ion's quantization axis (determined by the direction of the residual magnetic field) and the vector of the stray field gradient:

$$\Delta\nu_{\mathrm{quad}} \propto 3\cos^2\beta - 1. \tag{4}$$

The shift, which was not resolved at the 10^{-15} level, can be averaged to zero by switching the quantization axis between three orthogonal orientations [37]. To reduce the influence of short-term variations in the direction of the stray field gradient [7], the magnetic field was rotated after each extrapolation to zero intensity, corresponding to a 40 min interval. As the line strength of the clock transition is a function of the relative angles of the quantization axis, beam propagation vector and laser polarization vector, choosing three arbitrary orthogonal directions would risk selecting a direction in which the line strength was extremely low, requiring a large probe power to drive the transition and hence an increased ac-Stark shift. To prevent this, a set of fields was

found with reasonably high and near-equal line strengths ($\approx 30\%$). If it had not been necessary to average out the quadrupole shift, it would have been possible to reduce the magnitude of the ac-Stark shift by operating in the magnetic field direction with optimum line strength and making a corresponding reduction in the laser power. The uncertainty in the cancellation of the quadrupole shift due to inaccuracies in the orthogonality of the fields was estimated by analysis of the tensor component of the 467 nm ac-Stark shift. This has a similar functional dependence to the quadrupole shift, but with the angle of interest being between the polarization of the probe laser and the quantization axis. By comparing the relative magnitudes of the easily resolved tensor light shift in the three selected quantization axes against the angular dependence predicted by theory, it is possible to place a limit on how well the desired field directions were realized and hence their orthogonality. This led to a 10% fractional uncertainty on the quadrupole shift in each of the three directions, and was taken to be 10% of the statistical uncertainty on each data point since the shift was unresolved.

The magnetic field flux density B at the ion in each field orientation was determined by observation of the Zeeman splitting of the $\Delta m_F = \pm 1, \pm 2$ components of the 436 nm transition. In this way, the residual field was determined to be 20 (2) μT throughout the entire dataset for all three orientations. This value was then used to correct for the second-order Zeeman shift $\Delta\nu_B$ of the octupole transition through the relation [18]

$$\Delta\nu_B/\mathrm{mHz} = -1.72(3)B^2/\mu\mathrm{T}^2. \tag{5}$$

The contributions to the Zeeman shift and uncertainty from ac magnetic fields due to mains and other sources have been omitted as they are estimated to be much lower than the uncertainty on the dc shift.

The second-order Doppler shift arising from excess micromotion was measured by analysis of the depth of modulation of the rf-photon correlation signal [38, 39]. This also allowed an estimate to be made of the Stark shift from any residual rf field experienced by the ion, which can arise from either a displacement of the ion from the centre of the trap or a phase offset between the endcaps. The corresponding shifts attributable to intrinsic micromotion and secular motion are two orders of magnitude lower and have therefore been neglected.

The best estimate for the coefficient for the black-body Stark shift comes from using a calculated value for the polarizability of the $^2\mathrm{F}_{7/2}$ state [40] and an experimental measure of the dc-Stark shift of the 436 nm transition [41]. It is the uncertainty in this coefficient that dominates the uncertainty on this shift rather than uncertainties in the assumed 294 K temperature.

The frequency measurement has a gravitational redshift correction arising from the Yb ion being (75 ± 15) cm lower than the time-averaged height of the caesium atoms between the two interrogations (Ramsey time) of the caesium fountain.

Further systematic effects were considered that do not give rise to shifts at the uncertainty levels quoted in table 1. These included ac-Stark shifts from leakage of cooling and repumper laser beams through their shutters, phase chirp from the AOM used to shutter the 467 nm light and any offset in the steering of the clock laser frequency onto the line centre of the atomic transition.

Apart from the ion-related systematic frequency shifts, it is also necessary to consider uncertainty arising from the frequency measurement process. For most of the data-taking period, the transition frequency was measured simultaneously using two different frequency combs, which were referenced to a common maser-referenced rf synthesizer. The values obtained using

Table 1. Summary of the systematic shifts with their associated uncertainties, grouped into ion-related systematics and frequency measurement systematics. The statistical uncertainty is then added to give a final uncertainty. The individual uncertainties are quoted to two significant figures for clarity of presentation, but to avoid rounding errors the total has been evaluated from more precise values.

Source	Shift/10^{-15}	$\sigma/10^{-15}$
ac-Stark shift (467 nm)	0	0.49
Second-order Zeeman	−1.07	0.21
Black-body Stark	−0.23	0.11
Quadrupole shift	0	0.05
ac-Stark shift (370 and 639 nm)	0	0.04
Second-order Doppler	0	0.02
Gravitational redshift	−0.08	0.02
Servo error	0	0.02
Trapping rf-field Stark shift	−0.02	0.01
AOM phase chirp	0	0.01
Subtotal	−1.40	0.55
Cs fountain systematics	0	0.23
10 MHz distribution and rf synthesizer	0	0.10
50 m fibre frequency offset	0	0.04
Frequency comb	0	0.01
Subtotal	0	0.25
Statistical	0	0.86
Total	−1.4	1.0

the two combs agreed to within one part in 10^{17}, demonstrating that the combs themselves introduce negligible uncertainty. Any uncertainty introduced by the rf frequency distribution and synthesizer must also be accounted for. This is assessed by dividing the output of the rf synthesizer down to 10 MHz and comparing this signal with the original 10 MHz signal distributed from the hydrogen maser, and is found to result in a mean systematic frequency shift of less than one part in 10^{16} for the period of the measurements.

The probe laser is delivered to the frequency comb via an optical fibre of 50 m length. If the temperature of the fibre were drifting during the measurement period, this would lead to a first-order Doppler shift. The temperatures of the two laboratories are actively stabilized to better than 0.1 K. If a worst-case temperature drift of 0.2 K is assumed over each dataset (minimum 6 h) and an estimate of the thermal expansivity of the jacketed fibre [42] is used, this would correspond to a fractional frequency shift of 4×10^{-17} on the light received at the comb.

The systematic uncertainty arising from the caesium fountain primary standard itself was recently evaluated to be 2.3×10^{-16} [36]. After making the necessary corrections and including all uncertainties, the transition frequency is determined to be 642 121 496 772 646.22 (67) Hz, corresponding to a relative standard uncertainty of 1.0×10^{-15}. This is in good agreement with the previously published value [8] but has an uncertainty more than one order of

magnitude lower. This makes it one of the most accurately measured optical transition frequencies to date.

4. Summary and outlook

An improved absolute frequency measurement of the 467 nm electric octupole transition in a single ion of $^{171}Yb^{+}$ has been presented, with more than one order of magnitude lower uncertainty than the previously published value [8]. The improved statistical uncertainty is largely attributable to the ability to stabilize the laser to the atomic absorption, along with greatly improved reliability due to the replacement of the Ti:sapphire probe laser with a new diode-based system allowing stabilization to the clock transition for extended periods. Dead time in the interrogation cycle has been reduced by the introduction of polarization rotation on the cooling light, removing the need to switch off a large magnetic field that was required for laser cooling. The new probe laser has also enabled observation of a narrower clock transition linewidth and hence a reduced ac-Stark shift and associated uncertainty. Improved amplitude stability of the probe laser has allowed observation of coherent excitation of the transition, increasing signal-to-noise via increased excitation efficiencies.

The largest contribution to the uncertainty of this measurement is the level of statistical noise on the data. However, the overall uncertainty would not be greatly improved by acquiring more data because the uncertainty in the ac-Stark shift constitutes a large fraction of the systematic error budget. This shift and its uncertainty can be reduced by narrowing the observed linewidth even further [8]. Alternatively, the introduction of an interrogation scheme that produces a near-perturbation-free transition frequency could reduce the uncertainty on the shift by two to three orders of magnitude [43].

The uncertainty in the second-order Zeeman shift correction also makes a large contribution to the error budget. The magnetic field was observed to drift from week to week by about 1–2 μT. In future, the ion will be shielded from this drift in the ambient field by the introduction of a mu-metal shield around the trap. The uncertainty on the field would then be dominated by the uncertainty in the fits to the 436 nm Zeeman components, reducing it by one to two orders of magnitude. In addition, the introduction of an EOM for polarization rotation on the 935 nm transition would allow operation in even lower residual magnetic fields.

One of the limiting systematic uncertainties of the $^{171}Yb^{+}$ standard may be the black-body radiation shift of the clock transition, which is not easily measured. It can be reduced to negligible levels by cooling the trap to cryogenic temperatures [12]. In the case of $^{171}Yb^{+}$, it is the uncertainty of the shift coefficient that dominates the uncertainty. This could be improved by a direct measurement of the polarizability of the $^{2}F_{7/2}$ state, at which point the error would be dominated by knowledge of the thermal radiation profile. Imaging the trap in the thermal region of the IR spectrum or installing sensors within the vacuum system would allow identification of any hotspots, which could then be appropriately shielded or modified to minimize their temperature rise. Alternatively, since the 436 and 467 nm transitions experience the same thermal environment, a system has been proposed that combines the frequencies of the two transitions to produce a 'synthetic' frequency that can suppress this fractional shift to the 10^{-18} level [44].

With these further improvements, the systematic uncertainty for the $^{171}Yb^{+}$ standard could be reduced below 1×10^{-17}.

Acknowledgments

We thank Nils Huntemann, Christian Tamm and Ekkehard Peik for some useful discussions. We also thank Geoffrey Barwood for his critical reading of the manuscript and Hugh Klein and Guilong Huang for their contributions to the experiment. This work was supported by the UK National Measurement System Pathfinder Programme.

Note added in proof. Since the submission of this paper, the results of another, independent, measurement of the absolute frequency of the 467 nm transition has been made available [45]. The measured transition frequency is in excellent agreement with the value presented in this paper and, to our knowledge, these values demonstrate the best agreement between trapped ion optical frequency standards to date.

References

[1] Young B C, Cruz F C, Itano W M and Bergquist J C 1999 *Phys. Rev. Lett.* **82** 3799–802
[2] Jiang Y Y, Ludlow A D, Lemke N D, Fox R W, Sherman J A, Ma L S and Oates C W 2011 *Nature Photonics* **5** 158–61
[3] Margolis H S 2010 *Contemp. Phys.* **51** 37–58
[4] Champenois C, Houssin M, Lisowski C, Knoop M, Hagel G, Vedel M and Vedel F 2004 *Phys. Lett.* A **331** 298–311
[5] Matsubara K, Hayasaka K, Li Y, Ito H, Nagano S, Kajita M and Hosokawa M 2008 *Appl. Phys. Express* **1** 067011
[6] Chwalla M *et al* 2009 *Phys. Rev. Lett.* **102** 023002
[7] Tamm C, Weyers S, Lipphardt B and Peik E 2009 *Phys. Rev.* A **80** 043403
[8] Hosaka K, Webster S A, Stannard A, Walton B R, Margolis H S and Gill P 2009 *Phys. Rev.* A **79** 033403
[9] Margolis H S, Barwood G P, Huang G, Klein H A, Lea S N, Szymaniec K and Gill P 2004 *Science* **306** 1355–8
[10] Barwood G, Gill P, Huang G and Klein H 2007 *IEEE Trans. Instrum. Meas.* **47** 226–9
[11] Dubé P, Madej A A, Bernard J E, Marmet L, Boulanger J S and Cundy S 2005 *Phys. Rev. Lett.* **95** 033001
[12] Oskay W H *et al* 2006 *Phys. Rev. Lett.* **97** 020801
[13] von Zanthier J *et al* 2000 *Opt. Lett.* **25** 1729–31
[14] Wang Y H, Dumke R, Liu T, Stejskal A, Zhao Y N, Zhang J, Lu Z H, Wang L J, Becker T and Walther H 2007 *Opt. Commun.* **273** 526–31
[15] Chou C W, Hume D B, Koelemeij J C J, Wineland D J and Rosenband T 2010 *Phys. Rev. Lett.* **104** 070802
[16] Roberts M, Taylor P, Barwood G P, Rowley W R C and Gill P 2000 *Phys. Rev.* A **62** 020501
[17] Blythe P J, Webster S A, Hosaka K and Gill P 2003 *J. Phys. B: At. Mol. Opt. Phys.* **36** 981–9
[18] Hosaka K, Webster S A, Blythe P J, Stannard A, Beaton D, Margolis H S, Lea S N and Gill P 2005 *IEEE Trans. Instrum. Meas.* **54** 759–62
[19] Webster S, Godun R, King S, Huang G, Walton B, Tsatourian V, Margolis H, Lea S and Gill P 2010 *IEEE Trans. Ultrason. Ferroelectr. Freq. Control* **57** 592–9
[20] Gill P and Riehle F 2006 *Proc. 20th European Frequency and Time Forum (Braunschweig)* pp 282–8
[21] Dzuba V A and Flambaum V V 2008 *Phys. Rev.* A **77** 012515
[22] Dzuba V A, Flambaum V V and Marchenko M V 2003 *Phys. Rev.* A **68** 022506
[23] Lea S N 2007 *Rep. Prog. Phys.* **70** 1473–523
[24] Rosenband T *et al* 2008 *Science* **319** 1808–12
[25] Schrama C, Peik E, Smith W and Walther H 1993 *Opt. Commun.* **101** 32–6
[26] Berkeland D J and Boshier M G 2002 *Phys. Rev.* A **65** 033413

[27] Drever R W P, Hall J L, Kowalski F V, Hough J, Ford G M, Munley A J and Ward H 1983 *Appl. Phys.* B **31** 97–105
[28] Webster S A, Oxborrow M, Pugla S, Millo J and Gill P 2008 *Phys. Rev.* A **77** 033847
[29] Webster S A, Oxborrow M and Gill P 2007 *Phys. Rev.* A **75** 011801
[30] Dehmelt H 1975 *Bull. Am. Phys. Soc.* **20** 60
[31] Itano W M, Bergquist J C, Bollinger J J, Gilligan J M, Heinzen D J, Moore F L, Raizen M G and Wineland D J 1993 *Phys. Rev.* A **47** 3554–70
[32] Margolis H S, Huang G, Barwood G P, Lea S N, Klein H A, Rowley W R C, Gill P and Windeler R S 2003 *Phys. Rev.* A **67** 032501
[33] Tsatourian V, Margolis H S, Marra G, Reid D T and Gill P 2010 *Opt. Lett.* **35** 1209–11
[34] Walton B R, Margolis H S, Tsatourian V and Gill P 2008 *IET Optoelectron.* **2** 182–7
[35] Szymaniec K, Park S E, Marra G and Chalupczak W 2010 *Metrologia* **47** 363–76
[36] Li R, Gibble K and Szymaniec K 2011 *Metrologia* **48** 283–9
[37] Itano W 2000 *J. Res. Natl Inst. Stand. Technol.* **105** 829–37
[38] Siemers I, Schubert M, Blatt R, Neuhauser W and Toschek P E 1992 *Europhys. Lett.* **18** 139–44
[39] Berkeland D J 1998 *J. Appl. Phys.* **83** 5025–33
[40] Lea S N, Webster S A and Barwood G P 2006 *Proc. 20th European Frequency and Time Forum (Braunschweig)* pp 302–7
[41] Schneider T, Peik E and Tamm C 2005 *Phys. Rev. Lett.* **94** 230801
[42] Lagakos N, Bucaro J A and Jarzynski J 1981 *Appl. Opt.* **20** 2305–8
[43] Yudin V I, Taichenachev A V, Oates C W, Barber Z W, Lemke N D, Ludlow A D, Sterr U, Lisdat C and Riehle F 2010 *Phys. Rev.* A **82** 011804
[44] Yudin V I, Taichenachev A V, Okhapkin M V, Bagayev S N, Tamm C, Peik E, Huntemann N, Mehlstäubler T E and Riehle F 2011 *Phys. Rev. Lett.* **107** 030801
[45] Huntemann N, Okhapkin M, Lipphardt B, Weyers S, Tamm C and Peik E arXiv:1111.2446v1